# Chapter 4

# Mechanism of Hydrodenitrogenation over Carbide and Sulfide Catalysts

## 4.1. Introduction

The previous chapter presented the successful preparation of a new bimetallic oxycarbide catalysts, which exhibited a particularly high hydrodenitrogenation activity. However, little is known about the mechanism and nature of the active sites of this class of catalyst for hydrodenitrogenation reactions. This is the scope of the present chapter.

Hydrotreating is used to substantially reduce the sulfur, nitrogen, oxygen and aromatics content of petroleum feedstocks, and is one of the most important steps in refining [1,2,3,4,5]. More stringent environmental requirements and interest in the upgrading of heavy residual fractions have stimulated increasing attention on both hydrodenitrogenation (HDN) and hydrodesulfurization (HDS) processes. It has long been recognized that HDN is more difficult and more demanding than HDS, requiring more severe reaction conditions. However, HDN has historically been of little concern to refiners because the quantities of nitrogen compounds in conventional petroleum feedstocks were relatively small. This situation is changing due to the need for processing lower quality crudes. Heavier fuels require the removal of more nitrogen in order to reduce $NO_x$ emissions, to avoid poisoning of acidic catalysts, and to meet specifications of marketable products.

At the industrial level, HDN is performed using either Ni-Mo-S/$Al_2O_3$ or Co-Mo-S/$Al_2O_3$ as catalysts. The development of new catalysts that are selective to C-N cleavage and understanding of their catalytic behavior is an important goal and is the ultimate purpose of this research.

Transition metal carbide and nitride catalysts have excellent potential for use in hydrotreating reactions [6,7,8,9]. In particular, molybdenum carbide and nitride are more active than a commercial Ni-Mo catalyst for nitrogen removal from coal-derived liquids [10]. Not only are these materials more active, but they are also sulfur resistant. Bimetallic compounds formed from two different transition metals have enhanced HDN and HDS activity over their monometallic counterparts and a commercial sulfide catalyst [11,12].

In this work, we investigate the mechanism of the carbon-nitrogen bond cleavage step of primary amines over a Nb-Mo bimetallic carbide ($NbMo_2C$), the corresponding monometallic compounds, $Mo_2C$ and NbC, and a $MoS_2/SiO_2$ reference sulfide catalyst. For the sulfide, the support was chosen to be neutral silica in order to better probe the role of acidic sites in the reaction. As will be discussed in more detail below, the studies involved the use of a series of aliphatic amines. The results indicated that on both the carbides and the sulfide, the nitrogen removal step occurred by a β-elimination pathway. Furthermore, infrared studies with a probe molecule (ethylamine) showed that the elimination step involved the decomposition of a quaternary ammonium ion intermediate formed by the reaction of the amine with Brønsted-acidic sites on the surface. The decomposition likely proceeds by a push-pull mechanism involving a base, which we speculate is a surface sulfide species, and an acid, which we suggest is a sulfhydryl

group. The fact that the same mechanism was obtained for the carbides and the sulfide should be the result of a similar surface composition formed under reaction conditions. The following section will describe the importance of studying aliphatic amine reactivity and the various possible reaction mechanisms.

Aliphatic amines are very reactive and are not substantial constituents in the original feeds, but they are formed as intermediates during HDN of cyclic nitrogen compounds. For example, the HDN of pyridine proceeds via saturation of the heterocyclic ring followed by ring opening to *n*-pentylamine and subsequent removal of the nitrogen by deamination. Considerable savings in hydrogen and a better hydrocarbon product would be obtained if the catalytic activity for C-N bond cleavage could be enhanced. Therefore, it is important to examine the last step corresponding to the C-N bond cleavage of the primary amine.

The mechanism most often mentioned for amine removal reactions is the Hoffmann degradation [13]. This mechanism usually requires that the leaving nitrogen be quaternized, and the degradation is known to occur only with saturated hydrocarbons. The N removal step is either a β-elimination, involving a hydrogen of the carbon in the β position with respect to the nitrogen atom (Scheme 4.1) [14], or a nucleophilic substitution (Scheme 4.2) [14]. Under the experimental conditions required for HDN, the olefinic compounds formed in Scheme 4.1 can be readily hydrogenated, and the thiols formed in Scheme 4.2 can be easily transformed into hydrocarbons by hydrogenolysis of the C-S bond. Monomolecular mechanisms are also possible, depending on the nature and concentration of the base or nucleophile (Scheme 4.3) [15]. The only difference is

that the carbocation is formed before an elimination or nucleophilic substitution takes place.

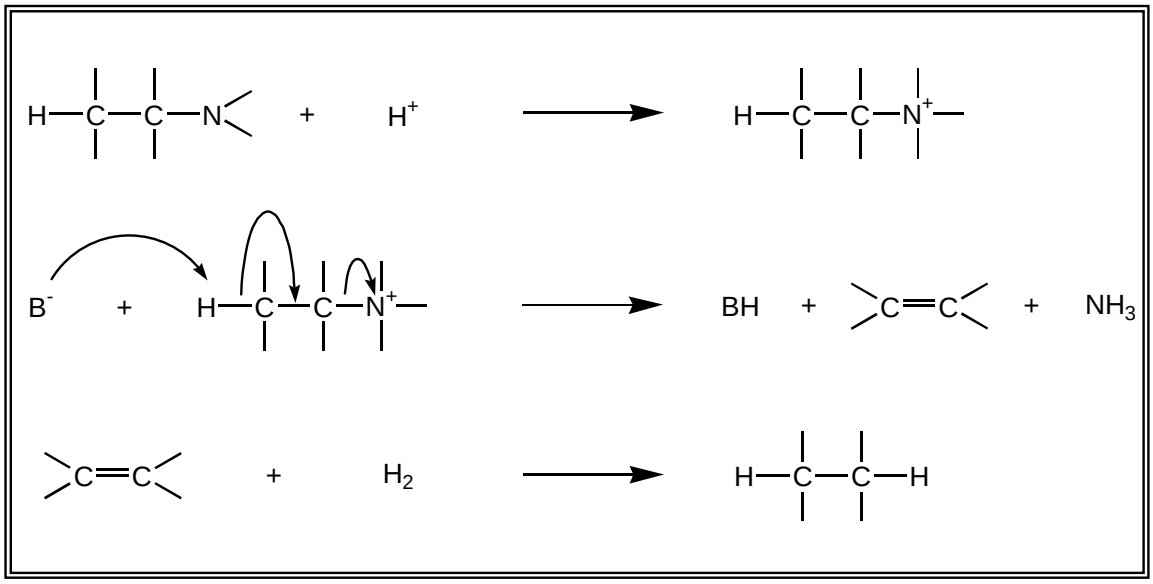

**Scheme 4.1.** β-Elimination

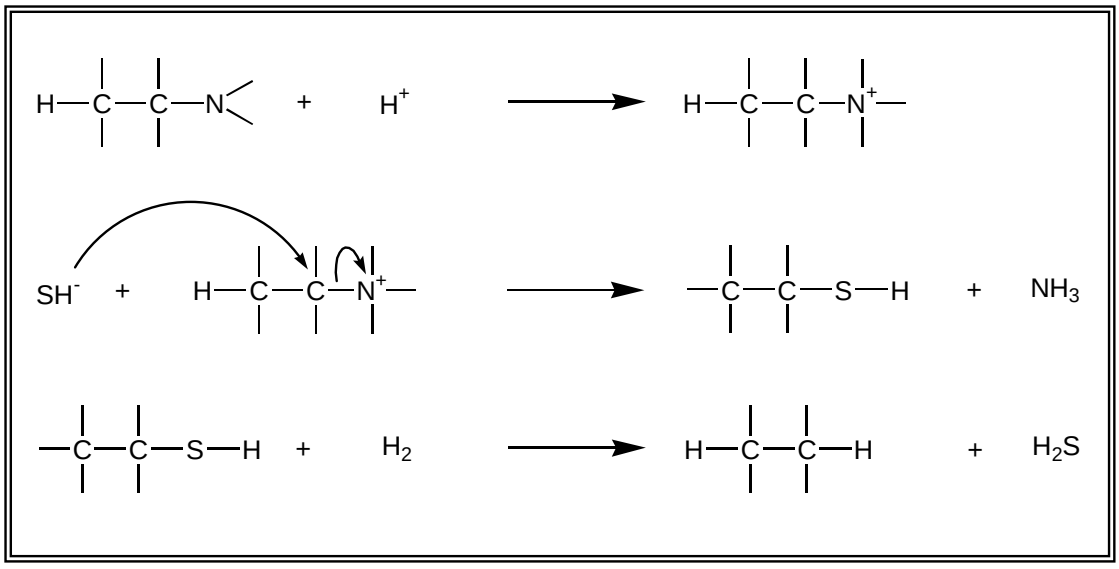

**Scheme 4.2.** Nucleophilic substitution

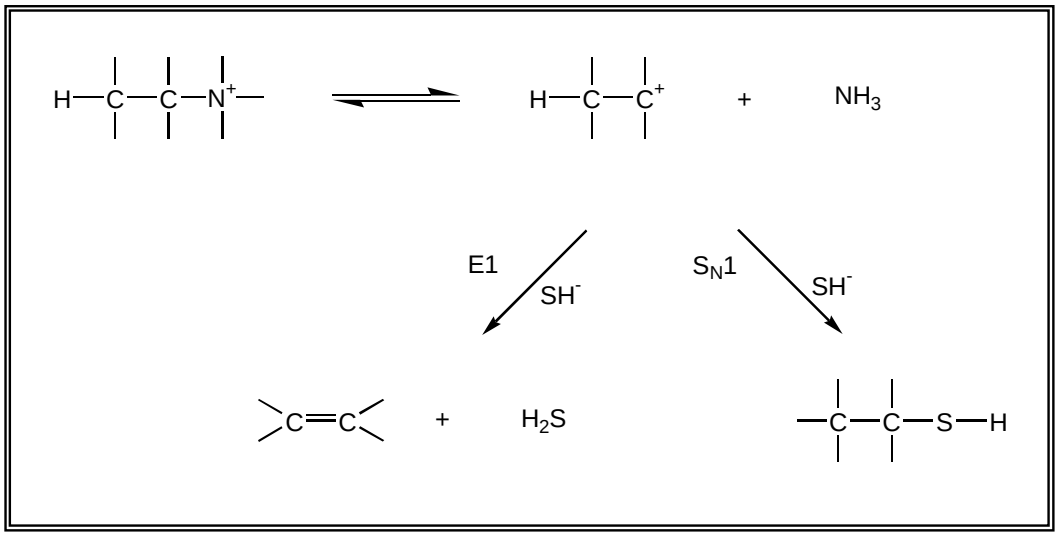


**Scheme 4.3.** E1 and $S_N1$

The base or nucleophilic agent required can be supplied by the amine itself or $H_2S$ via its dissociation on the catalytic surface. That is the likely reason $H_2S$ is found to promote C-N bond cleavage reactions [16,17,18,19].

Another mechanism, which involves metal atoms or ions and includes metal alkyl or metal alkylidine intermediates, has been proposed [20]. The mechanism can be considered as a metal-assisted displacement type of reaction, and likely is operative with metallic catalysts, such as iridium and osmium.

In order to distinguish between the mechanisms most often proposed, β-elimination and nucleophilic substitution, we have adapted the method developed by the group of Breysse [14,15,21]. However, we employed liquid-phase conditions at high pressure (3.1 MPa), whereas the original work was carried out in the gas phase at atmospheric pressure. The method consists of testing the reactivity of a series of amines (*n*-pentylamine, *tert*-pentylamine, *neo*-pentylamine), which have different structures and different numbers of hydrogen atoms on the carbon atoms in the α and β positions with

respect to the nitrogen atom. The expected reactivities depend on the mechanism proposed (Table 4.1) and are based on the following factors: a) the $S_N2$ mechanism depends on the steric hindrance of the carbon in the α position, b) the elimination mechanism cannot occur with *neo*-pentylamine and increases with the number of H atoms in the β position, and c) the monomolecular mechanism is preferred where the intermediate species involves a tertiary carbocation.

**Table 4.1**. Reactivities of different amines [ref. 15]

| Molecules<br>$X^-$ = strong base or nucleophile<br>C = amine carbon | **Possible mechanisms**<br>$S_N1$ : $X^- \curvearrowright C_\alpha^+$<br>$S_N2$ : $X^- \curvearrowright C_\alpha$<br>E1 : $X^- \curvearrowright C_\beta — C_\alpha^+$<br>E2 : $X^- \curvearrowright C_\beta — C_\alpha$ |
|---|---|
| I) 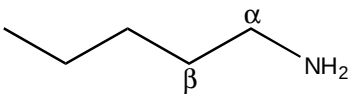 | $S_N2 > E2 >> S_N1 \approx E1$ |
| II) 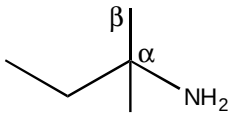 | $E1 > E2 \approx S_N1 >> S_N2$ |
| III) 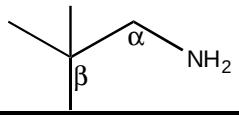 | $S_N2 > S_N1$ |

There is also a question about the involvement of acidity in the C-N bond scission, since as shown in Schemes 4.1 and 4.2, both β-elimination and nucleophilic substitution can be catalyzed by protons. It was earlier found that acid sites probed by $NH_3$ adsorption were not involved in the reaction of the amines on $Mo_2C$, $NbMo_2C$, and $MoS_2/SiO_2$ [22]. In this study, temperature programmed desorption (TPD) experiments and infrared spectroscopy of the gaseous base, ethylamine, were used to demonstrate that the HDN reaction of the amines proceeded by formation of quaternary ammonium species on Brønsted acid sites.

In summary, the reactivity of the three isomeric amines was tested under high pressure and liquid-phase over $Mo_2C$, NbC, $NbMo_2C$, and $MoS_2/SiO_2$. The carbide catalysts were synthesized by a temperature programmed reaction method and were characterized by CO chemisorption (or $O_2$ chemisorption), BET surface area measurements, X-ray diffraction (XRD), TPD and diffuse reflectance infrared Fourier transform (DRIFT) spectroscopy of ethylamine, and their reactivity for simultaneous HDN of quinoline and HDS of dibenzothiophene.

## 4.2. Experimental

### 4.2.1. Materials

Materials used for the preparation of the catalysts were: molybdenum (VI) oxide ($MoO_3$, 99.95%, Johnson Matthey), niobium (V) oxide ($Nb_2O_5$, 99.9%, Johnson Matthey), silica ($SiO_2$, Degussa) with surface area of 90 $m^2g^{-1}$, and $(NH_4)_6Mo_7O_{24}\cdot 4H_2O$ (Aldrich Chemical Co., A.C.S. reagent). The gases employed were He (Air Products, 99.999 %), $CH_4$ (Air Products, UHP Grade), $H_2$ (Air Products, 99.999%), $N_2$ (Air

Products, 99.999 %), 0.5% (v/v) $O_2$ / He (Air Products, 99.999%), 30 % $N_2$ / He (Air Products, 99.999%), CO (Air Products, 99.3 %), 10% (v/v) $H_2S/H_2$ (Air Products, 99.999%). For the reactivity tests, the chemicals employed were: dibenzothiophene (Aldrich, 99.5 %), quinoline (Aldrich, 99.9 %), benzofuran (Aldrich, 99.9 %), tetralin (Aldrich, 99.5 %) and tetradecane (Jansen Chimica, 99 %), *n*-pentylamine (Acros, 99 %), *tert*-pentylamine (Acros, 99 %), *neo*-pentylamine (TCI, 99 %), ethylamine (Aldrich, 97%), dimethyl disulfide (Aldrich, 99 %), octane (Acros, 99 %). All chemicals were used as received. $CH_4$, $H_2$, $N_2$ and 30% $N_2$/He were passed through water purifiers (Alltech, model # 8121) positioned in the line between the gas cylinders and the reactor, while He and CO were passed through a water/oxygen-removing purifier (Alltech, model # 8121 and 4004).

### 4.2.2. Synthesis of Catalysts

The synthesis of the bimetallic carbide involved two stages as described elsewhere [12]. Briefly, the first step consisted of the preparation of a bimetallic oxide precursor by the solid-state fusion of two monometallic oxides, $MoO_3$ and $Nb_2O_5$, at a metal ratio (Mo/Nb) equal to 2.0. The oxides were pressed at 8000 psi in a hard steel die, calcined at 1058 K for 6 hours, cooled to room temperature, and then ground to 16/20 mesh size. The second step involved the formation of the bimetallic carbide by the temperature programmed synthesis (TPS) from the bimetallic oxide with a 20% $CH_4/H_2$ gas mixture. The bimetallic oxide pellets were transferred to a quartz reactor, which was placed inside a tubular resistance furnace (Hoskins, 550 W), controlled by a temperature-programmer controller (Omega, Model CN2000). A 20% $CH_4/H_2$ gas mixture was passed through the oxide precursor at a flow rate of 273 μmol $s^{-1}$ (400 $cm^3$ $min^{-1}$) for a 0.7 g

batch. The temperature was increased linearly at a rate of $8.3 \times 10^{-2}$ K $s^{-1}$ (5 K $min^{-1}$) to a final temperature of 1063 K which was held for 1.5 h. Once the reaction was completed and the reactor was quickly cooled down to room temperature under He flow, the gas flow was switched to a 0.5% $O_2$/He gas mixture in order to passivate the carbide. Passivation of carbides is generally performed to avoid bulk oxidation of the samples when exposed to the atmosphere. The resulting bimetallic compound is denoted in this paper as $NbMo_2C$, to reflect the Nb/Mo ratio and the fact that it is a carbide. In fact, its composition is close to $NbMo_2O_{2.6}C_{4.7}$ [23] and has been denoted as NbMo-O-C in other publications [24,25].

For the preparation of the monometallic $Mo_2C$ and NbC, only the second carburization step was applied, with the corresponding single metal oxides being used as precursors. The temperature programs used for the carburization of each of these materials were obtained from optimized conditions found in the literature [26,27].

Two 5.5 wt % $MoS_2/SiO_2$ catalysts were used as the sulfide references, and were prepared in identical manner by flowing 100 μmol $s^{-1}$ (150 $cm^3$ $min^{-1}$, NTP) of 10% $H_2S/H_2$ over 5 wt % $MoO_3/SiO_2$ for 2 h at 673 K. The precursor $MoO_3/SiO_2$ was obtained by an incipient wetness technique, using an aqueous solution of $(NH_4)_6Mo_7O_{24}\cdot 4H_2O$ added dropwise to $SiO_2$. The impregnated sample was dried and calcined by heating at a low rate of 0.5 K $min^{-1}$ to a temperature of 773 K, which was held constant for 6 h and then lowered to room temperature.

### 4.2.3. Characterization

The catalysts were characterized by CO chemisorption ($O_2$ chemisorption for the sulfide catalysts), $N_2$ physisorption , X-ray diffraction (XRD), TPD and DRIFT of ethylamine, and their reactivity was measured for simultaneous HDN and HDS.

Prior to the adsorption measurements, the catalysts underwent standard pretreatment in a $H_2$ flow at 723 K for 2 h in order to remove the oxide layer formed during the passivation process. In the case of the sulfide catalysts, the standard pretreatment involved flowing a mixture of 10% $H_2S/H_2$ at 673 K for 2 h. CO or $O_2$ chemisorption was then measured to titrate surface metal centers on the catalysts to allow the calculation of nominal turnover rates and the comparison of catalytic activity. The chemisorption measurements were carried out right after the pretreatment without exposure of the catalysts to the atmosphere. Pulses of CO or $O_2$ gas were introduced through a sample valve with a carrier He gas stream while the effluent gas stream was sampled into a mass spectrometer (Ametek/Dycor Model MA100) chamber through a variable leak valve (Granville Philips Model 203). A computer recorded the mass signals of the effluent gas and the total uptake was calculated by referring the areas under the CO or $O_2$ mass signal peaks to a known quantity of injected CO or $O_2$. CO chemisorption was carried out at room temperature while $O_2$ chemisorption was done at dry ice temperature. At this temperature, it is found that corrosive chemisorption is minimized [28,29].

Surface areas were determined immediately after the gas chemisoption measurements by a similar flow technique using a gas mixture of 30% $N_2$ /He passed over the sample, which was kept at liquid nitrogen temperature. The amount of $N_2$ physisorbed

was estimated by comparing the desorption area to the area corresponding to the injection of a calibrated volume (34 μmol). The surface area was calculated from the single point BET equation.

TPD of the passivated samples was carried out following pretreatment with $H_2$, in the case of the carbide catalysts, and 10% $H_2S/H_2$, in the case of the sulfide catalysts. First, the uptake of ethylamine was measured using the same method as the one utilized for CO uptake. After saturation with ethylamine and purging in a He stream, the temperature was raised at a linear rate of $1.7 \times 10^{-1}$ K $s^{-1}$ (10 K $min^{-1}$) to 1273 K. The effluent from the reactor was sampled into a mass spectrometer to monitor species desorbed during the heating. The areas of the desorbed gases were compared to the area of calibrated gas pulses.

DRIFT spectra of ethylamine in the gas-phase and adsorbed on the carbide and sulfide catalysts were measured by means of diffuse reflectance using a Fourier transform infrared spectrometer (Bio-Rad Model FTS 60A). The catalysts, finely powdered, were placed in a high temperature environmental chamber (Spectra tech Model HTEC-0030-103) and following the standard pretreatment of each catalyst, the samples were exposed to ethylamine gas flow. IR spectral acquisition consisted of 1024 scans of the region 4000-400 $cm^{-1}$ at room temperature. The sample spectrum was normalized by the background spectrum acquired using a blank KBr sample. Spectra were recorded in the presence of the gas phase and after purging with He. The final spectra were calculated after subtraction from the one obtained before the catalysts being exposed to ethylamine. Additionally, for the carbide catalysts, spectra of the adsorbed ethylamine were obtained after the catalysts were exposed to a gas mixture of $H_2S/H_2$ corresponding to a

concentration of 3000 ppm of sulfur at 553 K. The goal was to reproduce the chemical environment, in which the catalysts were exposed during the reactivity tests, and verify any changes in the spectra.

Powder XRD patterns were acquired using a diffractometer (Scintag, Model XDS2000) with a $CuK_\alpha$ monochromatized radiation source, operated at 45 kV and 40 mA. The reactivity of all catalysts was tested for simultaneous HDN of quinoline and HDS of dibenzothiophene at 3.1 MPa and 643 K, in the same three-phase, trickle-bed reactor used for the aliphatic amine reactions.

### 4.2.4. Reactivity of Aliphatic Amines

The reactivities of the three amines (*n*-pentylamine, *tert*-pentylamine, and *neo*-pentylamine) were measured separately in the trickle-bed reactor, employing liquid phase conditions at 3.1 MPa and various temperatures. The reactivity unit consisted of three parallel reactors immersed in a fluidized sand bath (Techne, Model SBL-2). The temperature of the sand bath was controlled by a temperature programmer (Omega, Model 6051). The reactors were 19mm/16mm (OD/ID) 316 stainless steel tubes with a 13 mm ID stainless steel basket placed inside, which was used to hold the catalyst pellets supported between quartz wool plugs. A central hole in the basket was provided for a thermocouple to slide through the catalyst bed. Liquid feed from a reservoir was pumped into the reactor by high pressure liquid pumps (LDC Analytical, Model NCI-1105). The liquid reactant was pre-mixed with hydrogen before reaching the catalyst bed, and was delivered in concurrent upflow mode for good contacting. Prior to the catalytic test, the carbides were activated in flowing $H_2$, while the $Mo/SiO_2$ catalysts were sulfided with a 10% $H_2S/H_2$ gas mixture at standard conditions. For the testing an amount of catalyst

corresponding to 70 μmol of CO uptake (carbides) or atomic oxygen uptake (sulfides) were loaded in the reactor. For the amines work the amount of $MoS_2/SiO_2$ used corresponded to 56 μmol of atomic oxygen uptake. The feed composition consisted of 2000 ppm of nitrogen (amine), 2000 ppm of *n*-octane (internal standard) and 3000 ppm of sulfur (dimethyl disulfide) in a tetradecane solvent. The $H_2$ flow rate was 110 $\mu mols^{-1}$ (150 $cm^3$/min, NTP) and the liquid feed was introduced at a rate of 5 $cm^3\ h^{-1}$. Because of the low liquid rates and the good mixture provided by the hydrogen flow, the reactor operated as a CSTR.

For each change in conditions and reagent, the reaction system was allowed to run for 60 h in order to establish steady-state. Liquid samples were collected at regular intervals to verify the attainment of steady-state and an average of the values obtained was used for the calculation of conversion and product distribution. Recheck of catalytic activity at standard conditions was done after several changes in operating parameters and these demonstrated that no deactivation occurred. Overall continuous experiments were run for a period of several months for each catalyst. The liquid samples were analyzed off-line by gas chromatography (Hewlett-Packard, 5890 Series II) using a fused silica capillary column (CPSIL-5CB) and a flame ionization detector. A typical chromatogram of a liquid sample obtained from *n*-pentylamine reaction is shown in Figure 4.1. The reaction products were identified by GC-MS (VG Quattro, triple quadrupole, EI positive method) and the results of the identification were confirmed by the injection of standard compounds. Retention times of all possible reaction products were also obtained by injecting standards. The peak areas were converted to concentrations by the use of relative response factors, which were obtained by injecting

known concentrations of a mixture of *n*-octane (standard) and the compound of interest at the same conditions of analysis. The areas under the peaks of the octane ($A_{oct}$) and the compound of interest (A) were measured and the relative response factor of the compound, f, was calculated as follows [30]:

$$f = f_{oct} \times \left( \frac{A_{oct}}{A} \right) \times \left( \frac{w}{w_{oct}} \right)$$, where $w/w_{oct}$ is the weight ratio of the compound and *n*-octane and $f_{oct}$ is given an arbitrary value of 1.

Table 4.2 presents the retention time and relative response factor for each reagent and products identified. The effluent of the reactor was a mixture of gas and liquid which was separated by gravity in two holding vessels connected in series with the gas-phase vented through a back pressure regulator. Analysis of the gas-phase revealed the presence of the same light hydrocarbons found in the liquid-phase. Since only the analysis of the liquid phase was performed during the tests, vapor-liquid equilibrium curves [31] were used to obtain a correction factor for each of the $C_5$ hydrocarbons in order to take into account the products remaining in the gas-phase. Using this method the mass balance closed to about 100% ± 10%.

**Table 4.2.** List of retention times and relative response factors of all reagents and products.

| Compound | Retention time / min | Response factor |
|---|---|---|
| Dimethylpropane | 3.8 | 1 |
| 2-methyl-butane | 5.3 | 1 |
| 1-pentene | 5.7 | 1 |
| 2-methyl-1-butene | 5.9 | 1 |
| *n*-pentane | 6.1 | 1 |
| *Trans*-2-pentene | 6.4 | 1 |
| *cis*-2-pentene | 6.7 | 1 |
| 2-methyl-2-butene | 6.9 | 1 |
| *tert*-pentylamine | 14.3 | 1.46 |
| *neo*-pentylamine | 16.3 | 1.46 |
| *tert*-butylnitrile | 24.9 | 1.27 |
| pyridine | 25.1 | 1.49 |
| *n*-pentylamine | 25.4 | 1.41 |
| piperidine | 25.4 | 1.49 |
| dimethyldisulfide | 25.7 | — |
| octane | 31.1 | 1 |
| pentanethiol | 31.5 | 1.44 |
| Tetrahydro-2-methyl thiophene | 34.8 | 1.44 |
| tetrahydro-2H-thiopyran | 37.8 | 1.44 |
| di-neo-pentylamine | 40.5 | 1.21 |
| N-butylpiperidine | 42.2 | 1.21 |
| N-pentylpiperidine | 47.3 | 1.21 |
| dipentylamine | 47.7 | 1.21 |
| tetradecane | 55.4 | 1 |
| tripentylamine | 57.7 | 1.06 |

## 4.3. Results

The XRD pattern of the bimetallic oxycarbide (Figure 4.2) reveals a single phase material with peaks indicating a face-centered cubic metallic arrangement, similar to one of its parents (NbC), but different from the other ($Mo_2C$), which has a hexagonal closed-packed structure. The line-broadening of the X-ray peaks of the bimetallic oxycarbide indicates the presence of small crystallites.

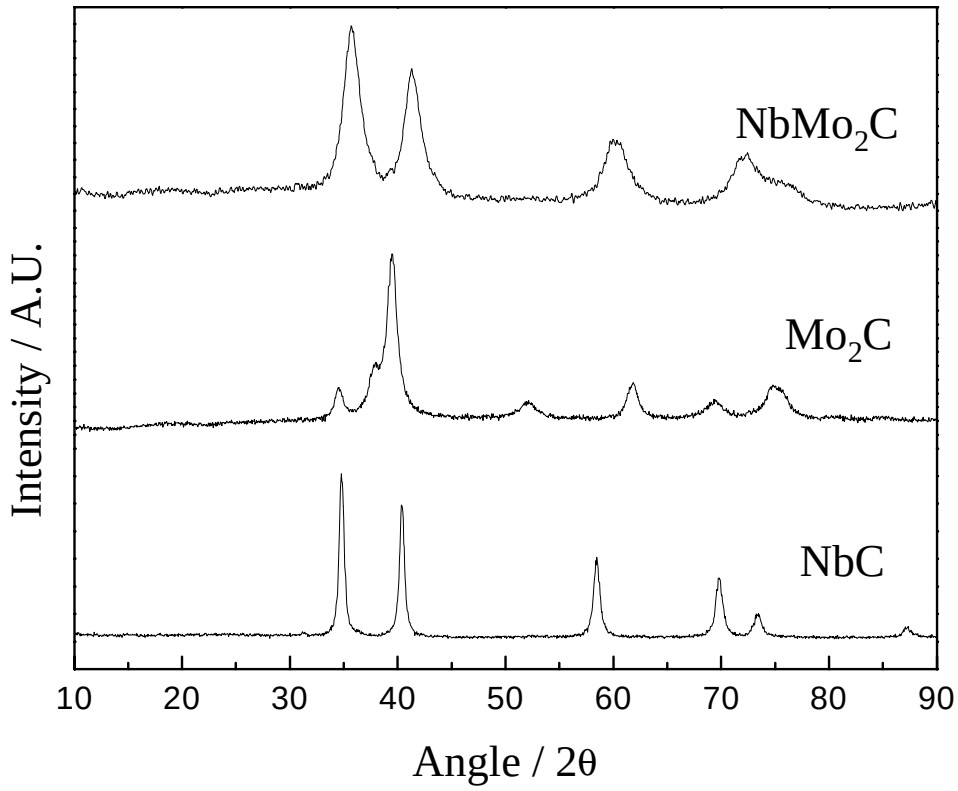


**Figure 4.2.** X-ray diffraction of Nb-Mo oxycarbide and its parent monometallic carbides.

A summary of the CO uptakes, surface areas and reactivity of each catalyst is presented in Table 4.3. $Mo_2C$ has the highest site density while NbC shows very low surface areas and CO uptake. The activity of the monometallic NbC for both HDN of quinoline and HDS of dibenzothiophene is very low, whereas the sulfide catalyst presents low reactivity for HDN of quinoline. The bimetallic carbide has a higher activity than the corresponding monometallic carbides, although activity varies with the ratio Mo/Nb [12].

**Table 4.3.** Characteristics of catalysts.

| | $Mo_2C$ | NbC | $NbMo_2C$ | $MoS_2/SiO_2$ |
|---|---|---|---|---|
| $S_A$ ($m^2$ $g^{-1}$) | 67 | 23 | 94 | 88 |
| CO uptake (μmol $g^{-1}$) | 106 | 5 | 25 | 17[c],27[d] |
| Site density ($\times 10^{15} cm^{-2}$) | 0.095 | 0.013 | 0.016 | 0.016 |
| % HDN (QNL)[a] | 47 | 5 | 57[b] | 10 |
| % HDS (DBT)[a] | 43 | 4 | 59[b] | 26 |

[a]Based on a catalyst amount equivalent to 70 μmol of CO uptake (carbide catalysts) and 70 μmol of atomic oxygen uptake (sulfide catalyst) loaded in the reactor. For NbC the values correspond to 30 $m^2$ loaded in the reactor (20 μmol) (ref.11). QNL = quinoline and DBT = dibenzothiophene. [b]Reactivity of a bimetallic with a composition of $NbMo_{1.75}$-O-C (ref. 12), which we believe has a similar crystal structure to the bimetallic prepared in this study. [c]Values based on the $O_2$ uptake, catalyst used for amines work. [d]Values based on $O_2$ uptake, catalyst used for QNL and DBT studies.

The reactivity of the aliphatic amines is presented as a function of temperature for the three catalysts, $Mo_2C$, $NbMo_2C$, and $MoS_2/SiO_2$ (Figure 4.3). All the values of conversion plotted in Figure 4.3 have an error in the range of ± 5% (high conversions) to ± 15% (low conversions). Because NbC showed the same catalytic activity as a blank reactor, the results for this catalyst are not presented. Conversion of *tert*-pentylamine was consistently higher for all three catalysts, while *neo*-pentylamine showed low conversion.

The product distributions for *n*-pentylamine for the three catalysts above are given in the left panels of Figure 4.4. The right panels show details of their C5 product distribution. For all catalysts, significant amounts of condensation species are observed as products of *n*-pentylamine reaction but their contribution diminishes with increasing temperature. The condensation species are a result of disproportionation reactions involving the parent amine with the most plentiful product being dipentylamine, but also small amounts of tripentylamine being formed. It can be seen that $Mo_2C$ produces a moderate amount of condensation products (Fig. 4.4a), $NbMo_2C$ a considerable amount (Fig. 4.4b), and $MoS_2/SiO_2$ the least (Fig. 4.4c). Pentanethiol is observed in small quantities for $Mo_2C$ and $MoS_2/SiO_2$ and is denoted "sulfur product" in Figure 4.4. The higher reactivity towards the C-S cleavage reaction is responsible for the low concentration of this species among the products. At higher temperatures and conversion levels, $C_5$ hydrocarbons are the predominant products, and their distributions are shown in the right panels of Figure 4.4. For $Mo_2C$ (Fig. 4.4a, right), *n*-pentane is preferentially formed among the $C_5$ hydrocarbons, followed by 1-pentene, *trans*-2-pentene, and *cis*-2-pentene. Compared to the formation of 1-pentene, a large amount of 2-pentene was

observed, indicating a significant double bond isomerization rate. For the $NbMo_2C$ catalyst (Fig. 4.4b), the right-side panel is omitted, because only *n*-pentane was found among the $C_5$ hydrocarbons. For this catalyst, the principal products observed were condensation species, but this was in part because only lower conversions were attained. For $MoS_2/SiO_2$ (Fig. 4.4c), conversions were the highest and the main product was found to be *n*-pentane, as in the case of $Mo_2C$.

The results of reaction of *tert*-pentylamine over the three catalysts are shown in Figure 4.5. Again, the left panels show conversion and overall selectivity and the right panels show details of the C5 product selectivity. The only products observed are saturated and unsaturated hydrocarbons (Figure 4.5). The thermodynamic equilibrium of the three hydrocarbons produced (2-methyl-2-butene, 2 methyl-1-butene, and 2-methyl-butane) was calculated for the temperature range and pressure of operation. The equilibrium constants for the reaction network were obtained from the values of the Gibbs free energy change. Correlation constants for the calculation of the free energy of formation for the individual compounds were taken from literature [32] and, after correcting for the operation pressure of 3.1 MPa, were used to determine the change in free energy for the reaction. The thermodynamic calculations indicated that the equilibrium lies well in the direction of complete formation of the saturated hydrocarbon (2-methyl-butane) at the experimental conditions employed in this study. Therefore, under such circumstances, the overall rate of hydrogenation of the unsaturated hydrocarbons is not controlled by thermodynamics but rather by kinetics for all the catalysts. The major difference between the sulfide and carbide catalysts is the higher selectivity for saturated hydrocarbons in the case of the sulfide.

The conversion and product composition for the *neo*-pentylamine reaction over the three catalysts is given in Figure 4.6. For $Mo_2C$ (Fig. 4.6a), formation of condensation products (dipentylamine) decreases with reaction temperature, while the amount of hydrocarbons (dimethylpropane) increases with temperature. At high temperatures a small amount of the dehydrogenation product, *tert*-butylnitrile, is detected. On $NbMo_2C$ (Fig. 4.6b), the only product observed was dipentylamine, but again, as in the case of the *n*-pentylamine reaction the temperature range used during this study led to lower conversions on this catalyst. On $MoS_2/SiO_2$ (Fig. 4.6c), the conversion levels are higher, but the results are similar to those for $Mo_2C$. Again, the condensation product, dipentylamine, decreases with increasing temperature, and the hydrocarbon, dimethylpropane, increases. Compared to $Mo_2C$, though, the selectivity for hydrocarbons products is lower at low conversions. Again, as with the case of $Mo_2C$ the dehydrogenation product, *tert*-butylnitrile was detected among the products.

At low temperatures formation of condensation products appears to be very selective and dipentylamine is the major product of the *n*-pentylamine and *neo*-pentylamine reactions. To investigate whether the disproportionation reaction equilibrium was established for the given operational conditions, equilibrium constants were calculated. The equilibrium constants for the reaction were obtained from the values of the free energy of formation for the individual compounds, which was calculated using a group contribution method (second order additivity method) [33]. Equilibrium conversions of pentylamine vary from 88 % at 473 K to 83 % at 553 K, both much greater than the observed conversions at those temperatures for all the catalysts. Thus,

although there is a high thermodynamic driving force for condensation product formation, particularly at low temperatures, equilibrium is not achieved.

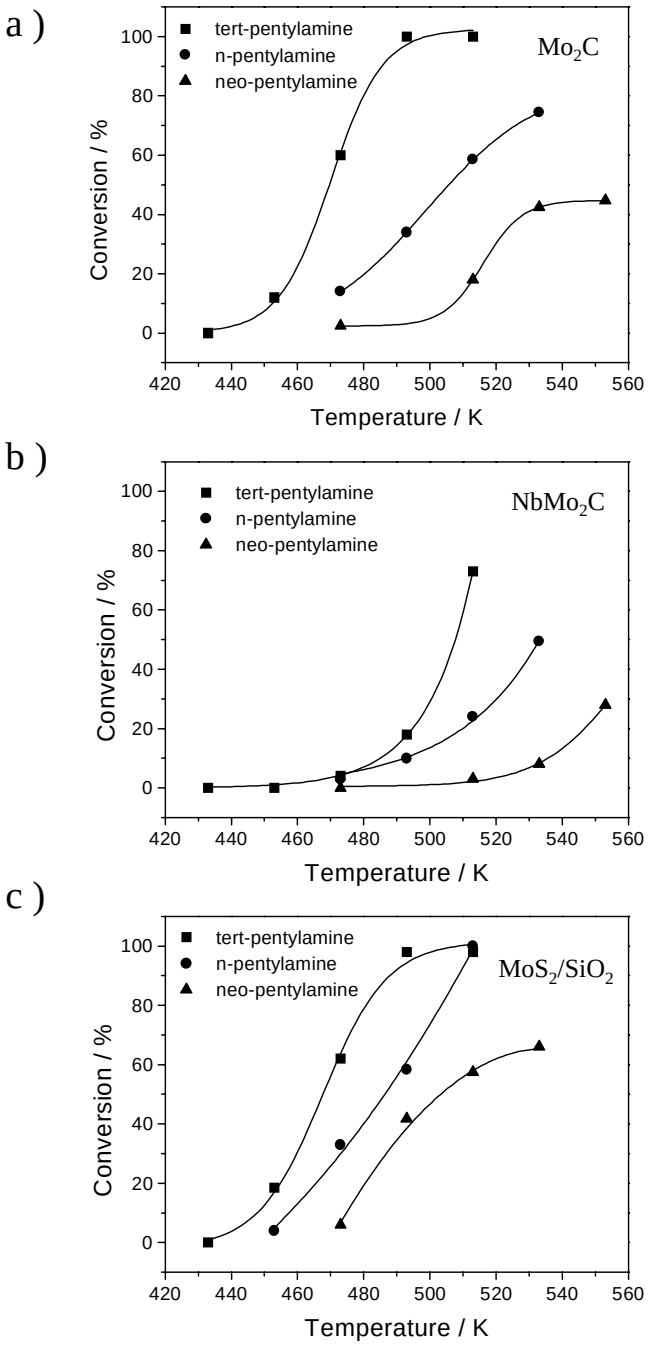


**Figure 4.3.** Conversion of *tert*-pentylamine, *n*-pentylamine, and *neo*-pentylamine over: a) $Mo_2C$; b) $NbMo_2C$; c)$MoS_2/SiO_2$.

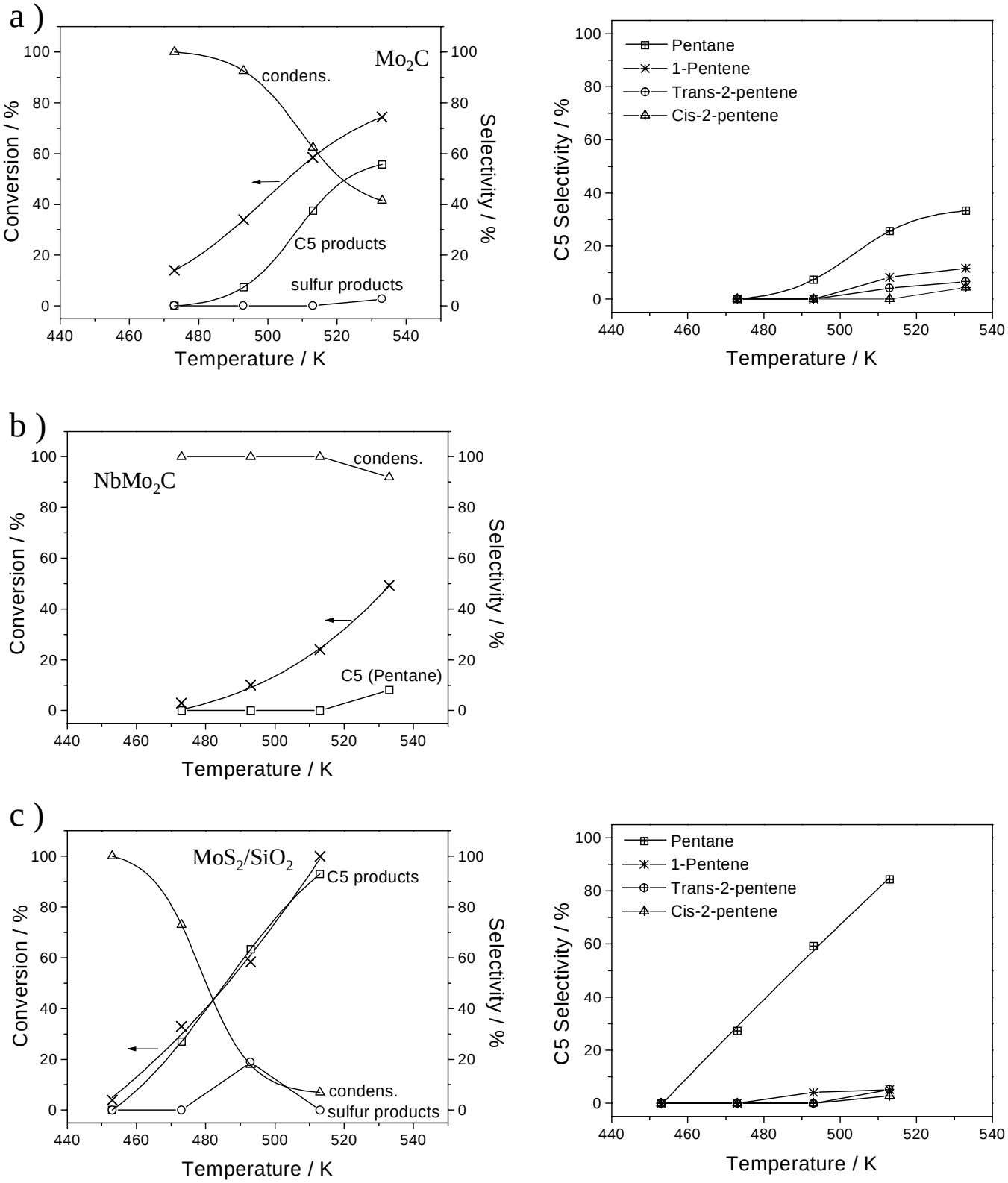


**Figure 4.4.** Conversion and product distribution for the *n*-pentylamine reaction over: a) $Mo_2C$; b) $NbMo_2C$; c)$MoS_2/SiO_2$.

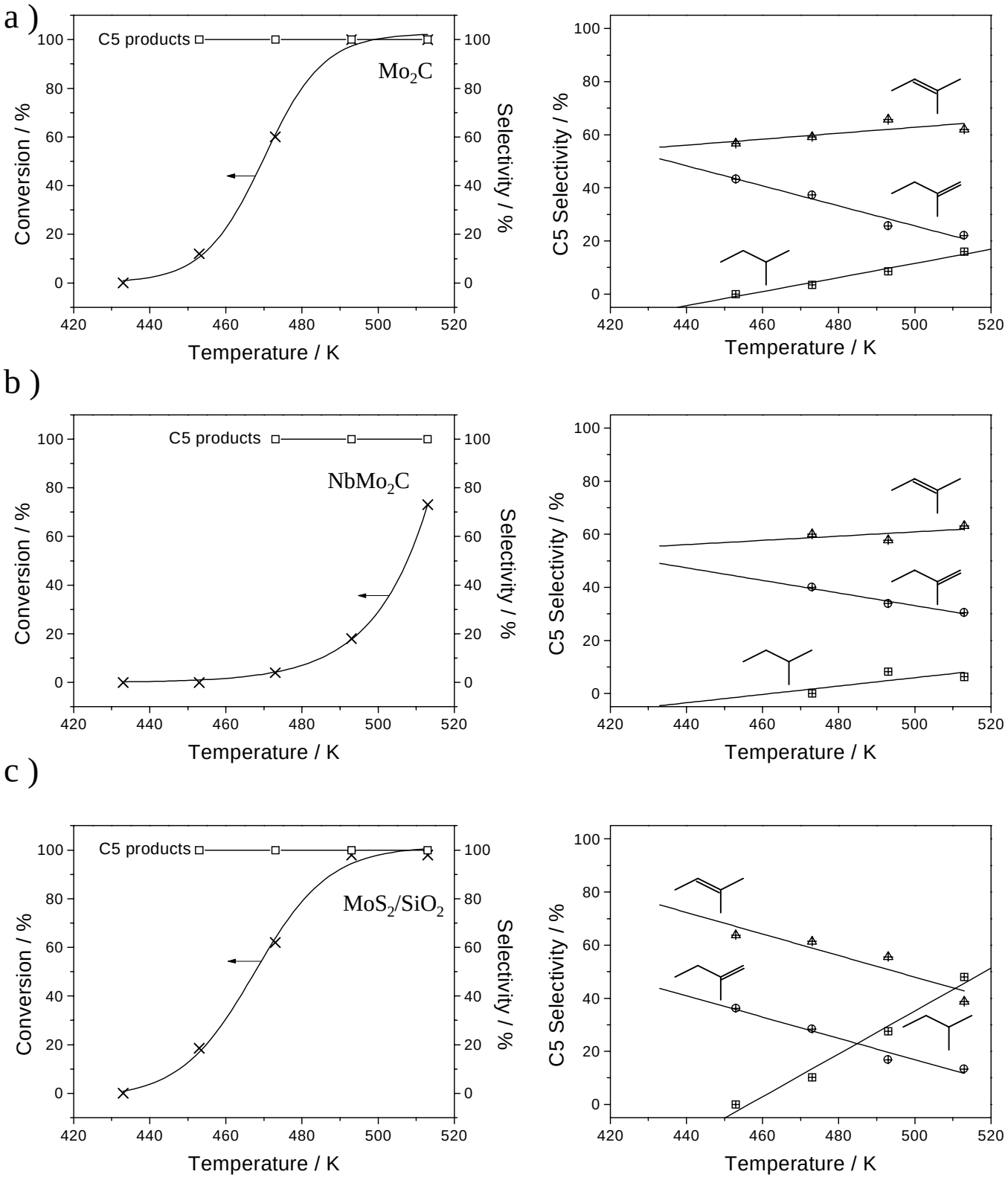


**Figure 4.5.** Conversion and product distribution for the *tert*-pentylamine reaction over: a) $Mo_2C$; b) $NbMo_2C$; c)$MoS_2/SiO_2$.

a )

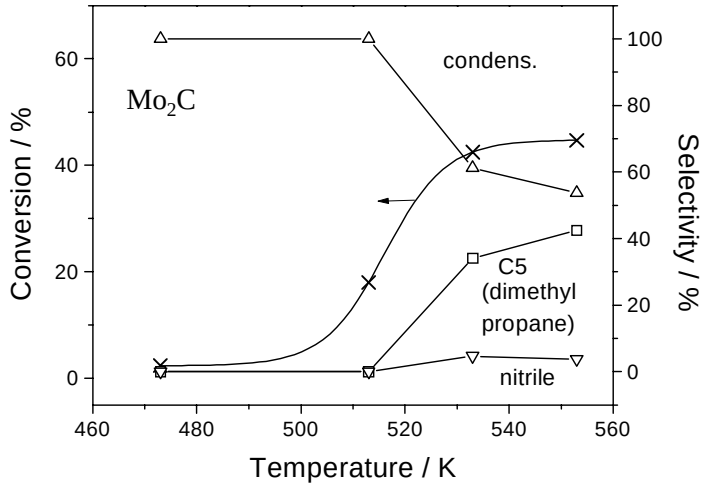


b )

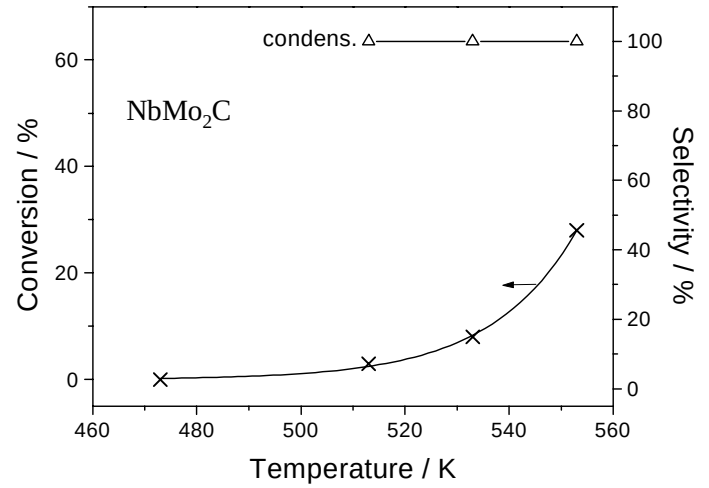


c )

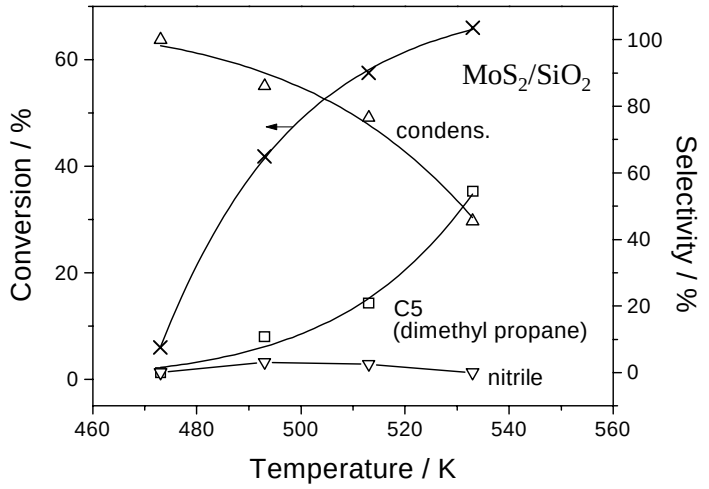


**Figure 4.6.** Conversion and product distribution for the *neo*-pentylamine reaction over: a) $Mo_2C$; b) $NbMo_2C$; c)$MoS_2/SiO_2$.

The TPD results for ethylamine on the three different catalysts are shown in Figure 4.7. In all cases, the desorption of unreacted ethylamine (m=30) and the products of elimination, ethylene (m=28) and ammonia (m=17), were observed. Unreacted ethylamine was observed at low temperatures in quantities of 55 μmol $g^{-1}$ for $Mo_2C$, 104 μmol $g^{-1}$ for $NbMo_2C$ , and 110 μmol $g^{-1}$ for $MoS_2/SiO_2$. The ratio of ethylene and ammonia desorbed was 1.0 ± 0.2. On the sulfide catalyst, all of those species desorbed at the same temperature, 383 K, and the desorption curves consisted of a single peak. On the carbide catalysts, the ethylene and ammonia curves consisted of multiple features, and the temperatures of desorption were equal or higher than the temperature of desorption of unreacted ethylamine. The total quantity of adsorbed ethylamine obtained by pulse adsorption minus the amount of desorbed ethylamine corresponded closely to the quantity of reaction products, ethylene and ammonia, as expected. The latter quantity is a measure of the number of Brønsted-sites [34,35,36], and these varied with the catalyst: 308 μmol $g^{-1}$ for $Mo_2C$, 209 μmol $g^{-1}$ for $NbMo_2C$ , and 258 μmol $g^{-1}$ for $MoS_2/SiO_2$.

The IR spectra for adsorbed ethylamine were identical for all catalysts and were consistent with the formation of adsorbed ethylammonium ions (Figure 4.8). It has been shown in other work that the NH stretching modes for the ethylammonium ion are the dominant features, whereas the CH stretching bands are the most intense features for ethylamine [34,37,38,39]. The presence of the ethylammonium ion is characterized by broad and intense features due to NH stretching in the region of 3000-3300 $cm^{-1}$ and weak CH vibrational modes between 2800-3000 $cm^{-1}$. The ethylamine IR spectra consist

of very intense CH vibrational bands between 2800-3000 $cm^{-1}$ and weak NH stretching modes between 3300-3450 $cm^{-1}$.

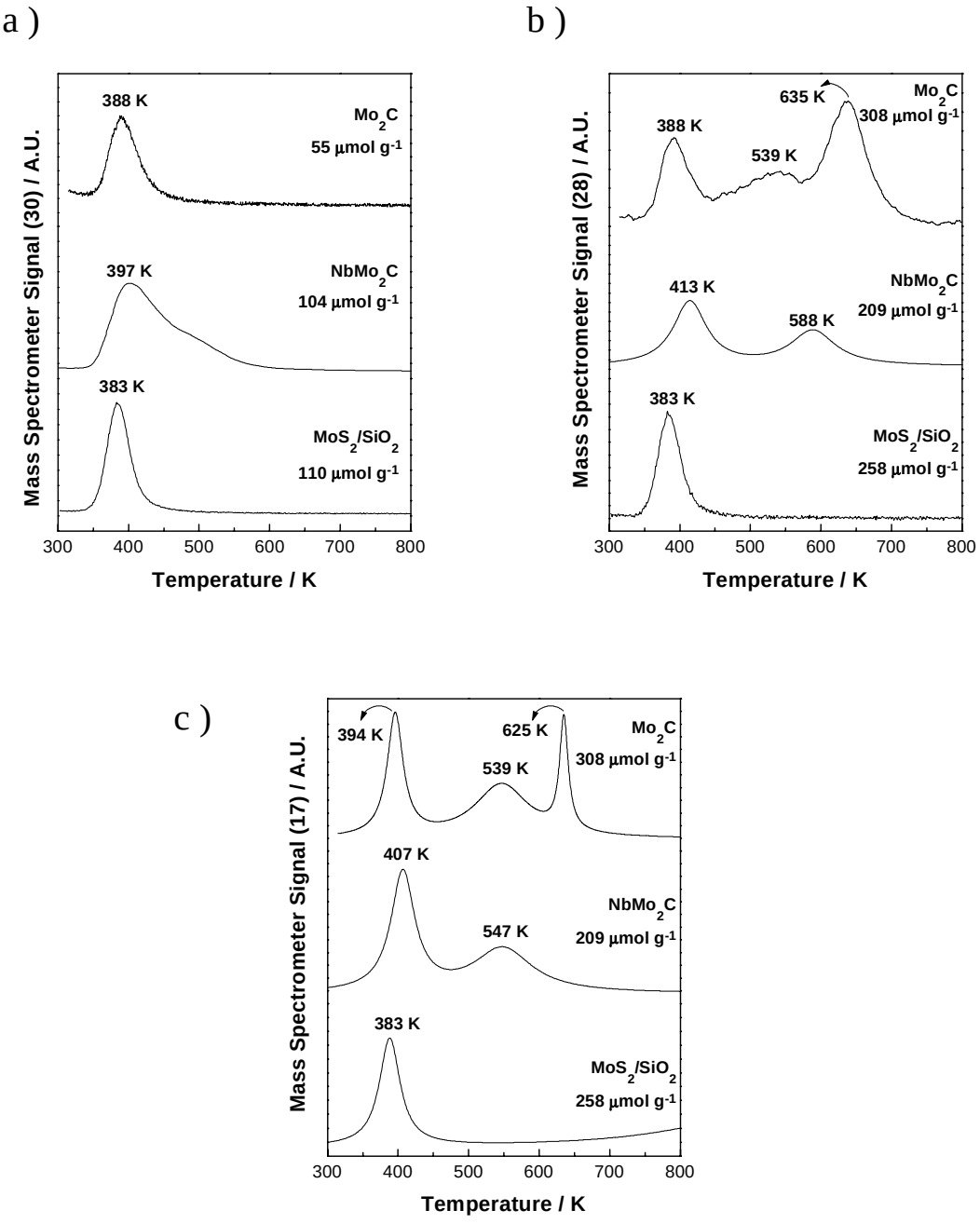


**Figure 4.7.** TPD curves for ethylamine in $Mo_2C$, $NbMo_2C$, and $MoS_2/SiO_2$: a) ethylamine (m=30), b) ethylene (m=28), and c) ammonia (m=17) were observed during the desorption.

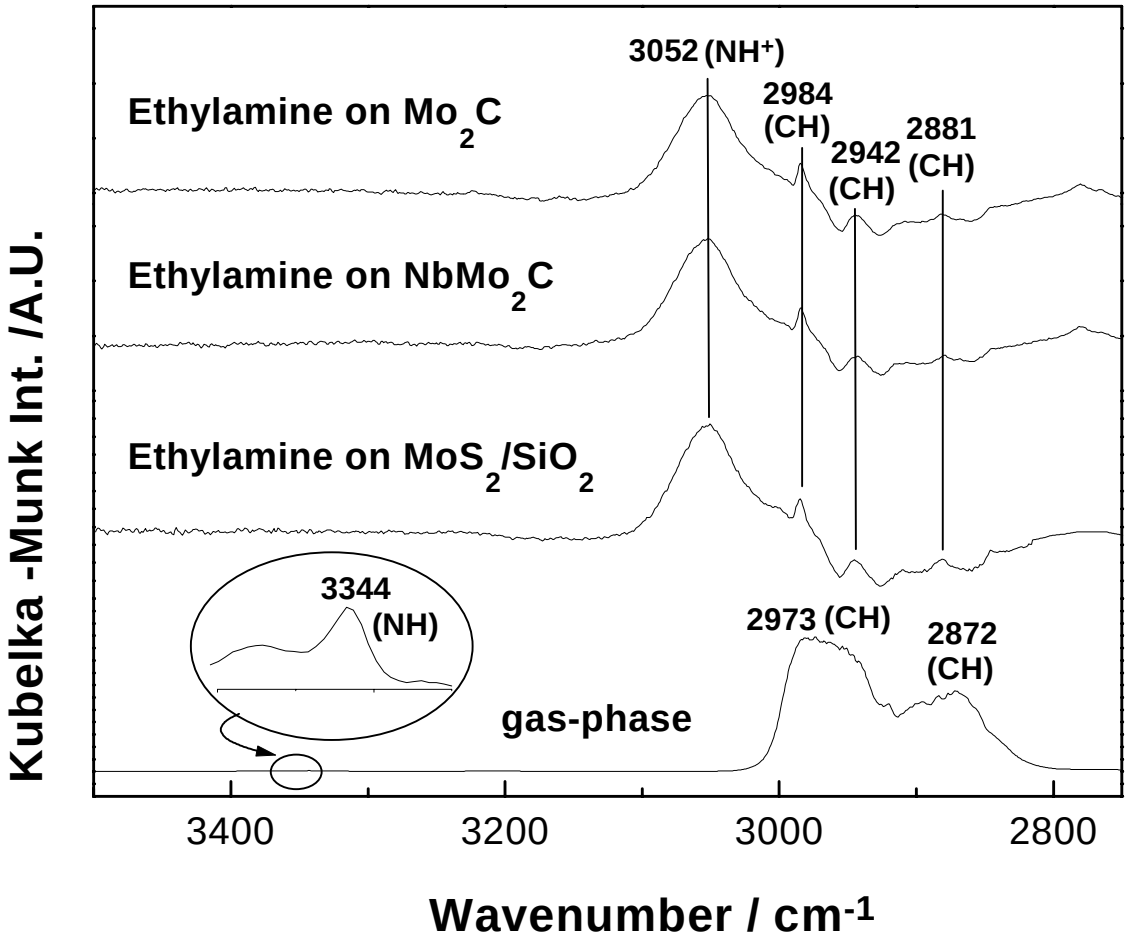


**Figure 4.8.** Comparison of the DRIFT spectra of ethylamine in the gas-phase and adsorbed on $Mo_2C$, $NbMo_2C$, and $MoS_2/SiO_2$.

## 4.4. Discussion

As seen from the sequence of reactivity of the aliphatic amines presented in Figure 4.3, for all catalysts *tert*-pentylamine is the most reactive amine, *n*-pentylamine is intermediate, and *neo*-pentylamine is the least reactive. This experimental observation is in consistent with an E2 elimination mechanism (Table 4.1).

The product distribution obtained from *n*-pentylamine (Figure 4.4) is consistent also indicates the contribution of a nucleophilic substitution pathway (Scheme 4.2). The major product is *n*-pentane, which is likely formed by the rapid hydrogenation of 1-pentene. The primary E2 product is 1-pentene, the most abundant olefin formed. The isomers *cis*- and *trans*-2-pentene are always found as minor products at larger conversions, indicating that they are formed from secondary isomerization reactions. The lack of branched isomers rules out the E1 mechanism, because a carbocationic intermediate (Scheme 4.3) would be expected to isomerize readily. The formation of condensation products and thiols can be explained by a parallel nucleophilic substitution mechanism. In the case of condensation products, the nucleophilic entity is the amine itself, while in the formation of thiols in the presence of $H_2S$, the nucleophile is hydrogen sulfide. Similar products have been observed in a number of previous studies in the literature using sulfide and oxide catalysts [14,15,40,41,42].

The product distribution obtained from *tert*-pentylamine (Figure 4.5) shows only hydrocarbons, suggesting an E2 mechanism. No condensation products were detected from *tert*-pentylamine as expected, due to steric hindrance around the carbon bearing the $NH_2$ group. The sulfide catalyst presented a better hydrogenation function than the

carbides as evidenced by the highest selectivity to the saturated hydrocarbon. The invariably higher concentration of 2-methyl-2-butene over 2-methyl-1-butene occurs because the preferred product in the elimination mechanism is the alkene that has the greatest number of alkyl substituents on the double bond.

The product distribution obtained from *neo*-pentylamine (Figure 4.6) consists mainly of high concentrations of condensation products at lower conversion levels, which should be formed by a $S_N2$ nucleophilic substitution mechanism, and a saturated hydrocarbon, dimethylpropane, formed at higher conversions. The only hydrocarbon formed from *neo*-pentylamine was a saturated one since the presence of unsaturated hydrocarbons is related to elimination-type mechanisms, which cannot occur when no hydrogen atoms are bonded to the β carbon (Table 4.1). $Mo_2C$ presented a particularly high selectivity for dimethylpropane when compared to the other catalysts. The dehydrogenation reaction of the amine into isobutylnitrile was only observed with *neo*-pentylamine as reactant, and then only in very small amounts (Figure 4.6). Cattenot *et al.* [15] reported the formation of nitriles from *n*-pentylamine over sulfide catalysts, while Sonnemans *et al.* [40] observed a dehydrogenation type of reaction only at $H_2$ pressures lower than 29 atm.

At low temperatures, only disproportionation into dipentylamines takes place when either *n*-pentylamine or *neo*-pentylamine is the reactant (Figures 4.4 and 4.6). In general, hydrocarbons are formed in larger amounts than condensation products at increasing temperatures and conversions, which is in agreement with the results obtained from the literature [15,40,41]. This is an interesting result since all other works cited were carried out under gas-phase conditions, in contrast with the liquid-phase conditions

used in this study. The preference towards condensation products at low temperatures is due to thermodynamics, as indicated by our calculations.

Noteworthy is the similarity between the $Mo_2C$ and $MoS_2$ catalysts regarding activity and product distribution in the amines reactions. This is probably because the active surface of both the carbide and sulfide are similar in composition at reaction conditions. On carbides, measurements of surface composition after reaction and studies with well-defined reference compounds have established that the active surface incorporates sulfur [43,44] and could be a carbosulfide [45]. On sulfides, studies by high resolution electron microscopy have indicated the presence of a carbide phase on the reactive surface [46]. Thus, regardless of the starting material, at reaction conditions there is a convergence in the composition of the active phase, with both carbon and sulfur being important components. The relative amounts of these species are likely determined by the nature of the feed and the reaction conditions. The implication of a common carbosulfide phase in hydroprocessing catalysts does not mean that the starting composition is not important. The underlying structure is likely to exert an indirect but strong influence on the reactivity of the external layer.

In summary, the nature of the products obtained for all catalysts analyzed (Figures 4.4-4.6) is consistent with two mechanisms, an elimination pathway leading to the formation of saturated and unsaturated hydrocarbons, and a nucleophilic substitution pathway, resulting in the production of dipentylamines and thiols. However, the observed increase in the rate of formation of denitrogenated products when going from *neo*-pentylamine to *n*-pentylamine and *tert*-pentylamine indicates that the main HDN mechanism operative on all catalysts is the elimination mechanism. The increase of

conversion corresponds to the increase in the number of hydrogen atoms bound to the carbon atom in the β position, suggesting that the removal of the hydrogen on the $C_\beta$ is the key step during denitrogenation. The nature of the base and the structure of the amine will determine if the amine will undergo either monomolecular (E1) or bimolecular (E2) elimination mechanism. In the first case, the base has limited influence on the kinetics; stronger or weaker, the base must wait until the carbocation is formed. In the second case, the properties of the base will impact the rate strongly; a stronger base will pull the hydrogen away from the substrate faster [47]. As discussed above, the hydrocarbon product distributions indicate that the operative mechanism here is of the E2 type.

Results obtained by others [14,15,48] about the preferred mechanism during the C-N bond cleavage step of the hydrodenitrogenation using diverse probe molecules show that the mechanism is strongly related to the catalyst and the structure of the N-containing molecule. The results of Vivier *et al.* [48] for the hydrodenitrogenation of 1,2,3,4,-tetrahydroquinoline and 1,2,3,4-tetrahydroisoquinoline over a sulfided commercial $NiMo/Al_2O_3$ catalyst suggest the occurrence of a nucleophilic substitution mechanism, while those of Portefaix *et al.* [14], using aliphatic amines over the same catalyst, indicate the operation of an elimination mechanism. Cattenot *et al.* [15] studied a series of sulfide catalysts and found that the mechanism depended on the catalyst studied.

Sulfide catalysts have been extensively studied, and much work has been carried out to understand the nature of the catalytic active centers for HDN. The existence of two distinct sites for hydrogenation and hydrogenolysis has been suggested [49,50]. Hydrogenation sites would occur on surface vacancies and would be transformed into weak acid centers (hydrogenolysis sites) following the dissociative adsorption of $H_2S$.

The HDN mechanisms presented in the introduction (Schemes 4.1-4.3) are incomplete in that they do not include the catalyst. In this study, identification of the reaction intermediate was carried out using the DRIFT technique in conjunction with TPD results to be described presently. The spectra obtained for ethylamine adsorbed on each catalyst and illustrated on Figure 4.8 for the $Mo_2C$ catalyst indicated the presence of an ethylammonium ion as an intermediate. The main feature at 3052 $cm^{-1}$ is assigned to the broad and intense NH stretch of an ethylammonium species [37,38,39]. Therefore, in the HDN reaction, the amine would first coordinate to a Brønsted-acidic site, forming a quaternary ammonium ion and then undergo a deprotonation by surrounding $S^{-2}$ entities adsorbed on anionic vacancies. A description of the mechanism is shown in Scheme 4.4 for a sulfide-type catalyst. The essence of the mechanism is a push-pull process by sulfur centers with basic character and putative $S^{+}$–H centers with Brønsted-acidic character. This can neatly explain the observed olefin distribution in the HDN of all the pentylamines. The preferred pathway is β-elimination and the products obtained depend not only on the thermodynamic stability of the product olefin but also on the availability and number of β-hydrogens. It should be pointed out that the surface structural features presented in Scheme 4.4 are not unique and other arrangements are possible. However, it does include elements like surface vacancies and sulfhydril groups which have been identified as being important on sulfide catalysts in a number of studies [15,42,51].

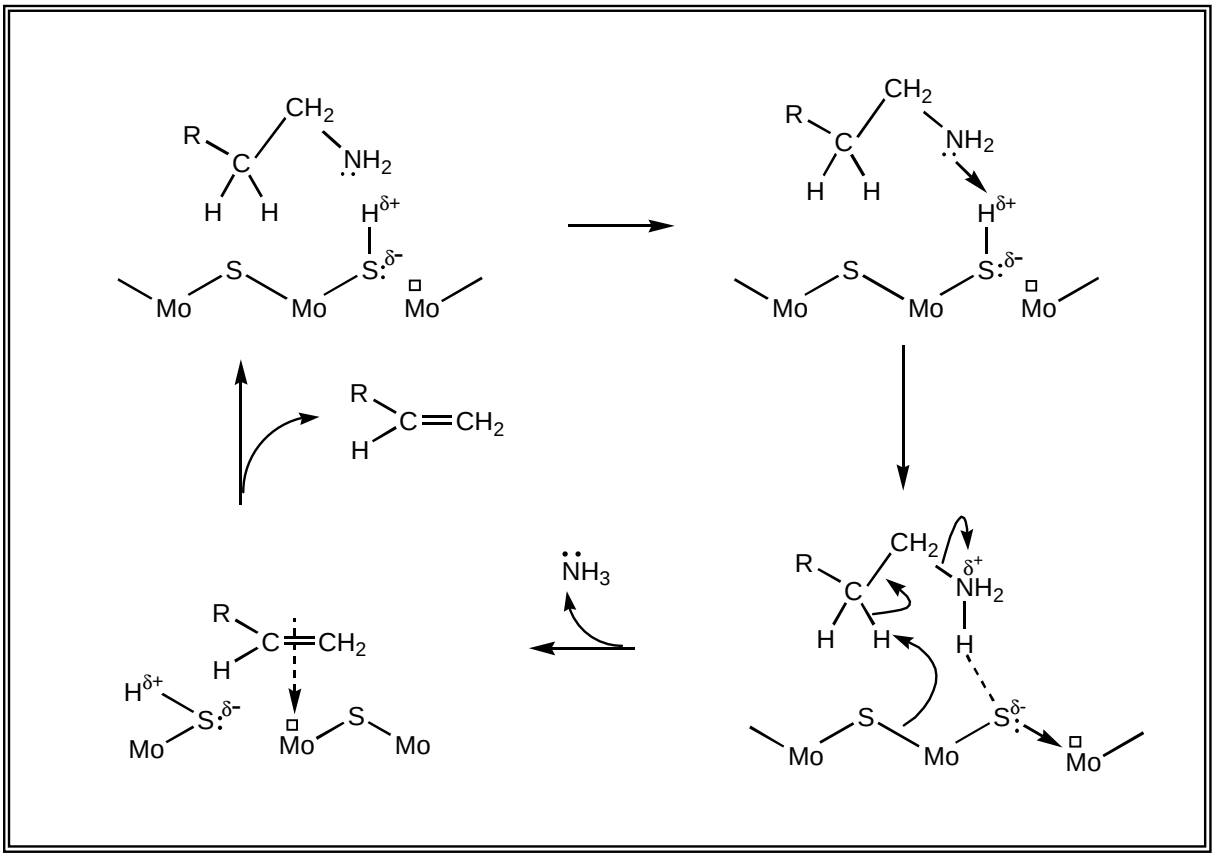


**Scheme 4.4.** Mechanism proposed for the HDN of a pentylamine.

TPD experiments of ethylamine served several purposes: 1) to find a correlation between acidity and activity, 2) to investigate the nature of the acid sites which catalyze the C-N bond cleavage reaction, 3) to identify the reactive intermediate. It has been demonstrated that TPD of ethylamine is particularly useful for the differentiation of Lewis and Brønsted acid sites [34,35,36]. This technique is based on the fact that the ethylammonium ions formed upon adsorption of the amine on the Brønsted acid sites, decompose via the β-elimination reaction to ethylene and ammonia (Scheme 4.2), whereas the amines associated with Lewis acid sites desorb unreacted. In our work it was found that indeed, the quantity of desorbed ethylene was equal to that of ammonia (1.0 ±

0.2) consistent with a β-elimination. Interestingly, although for the sulfide the desorption peaks for these species coincide, for the carbides the ethylene peak tended to appear after the ammonia peak. This suggested that for the sulfide the β-elimination occurred with concurrent ethylene and ammonia release, whereas for the carbides the ethylene was retained, probably by interaction with a molybdenum vacancy site. This is accounted for in Scheme 4.4. As discussed above, the quantity of ethylamine converted into ethylene or ammonia during the TPD of ethylamine, should relate to the number of Brønsted sites. The difference of ethylamine adsorbed and ethylamine desorbed during the TPD is also equivalent (1 ± 0.2) to the quantity of ethylene and ammonia desorbed. With the present catalysts it was found that the latter varied in the following order: $Mo_2C$ > $MoS_2/SiO_2$ > $NbMo_2C$ (Figure 4.7). The same trend was found for the specific rate of *tert*-pentylamine reaction (Figure 4.9). The molecule, *tert*-pentylamine, is particularly appropriate for this comparison, since, on all catalysts, it seems to react only through a β-elimination leading exclusively to hydrocarbons.

A similar push-pull type of mechanism can be invoked to explain the isomerization of olefins (Scheme 4.5). No carbocations are formed, so no isomerization of the hydrocarbon chain occurs. Thus, *n*-pentylamine produces only normal olefins. The push-pull mechanism can also be readily extended to saturated heterocycles (Scheme 4.6). Only the first step is shown in the scheme, subsequent deamination can occur on adjacent sites as in Scheme 4.4. What can be inferred for heterocycles from this simple mechanism is that the site requirements are more stringent. This suggests that the reactivity behavior for heterocycles may be considerably different from that of simple

amines considered here. As will be mentioned later, this is indeed the case for the HDN of quinoline on these same catalysts.

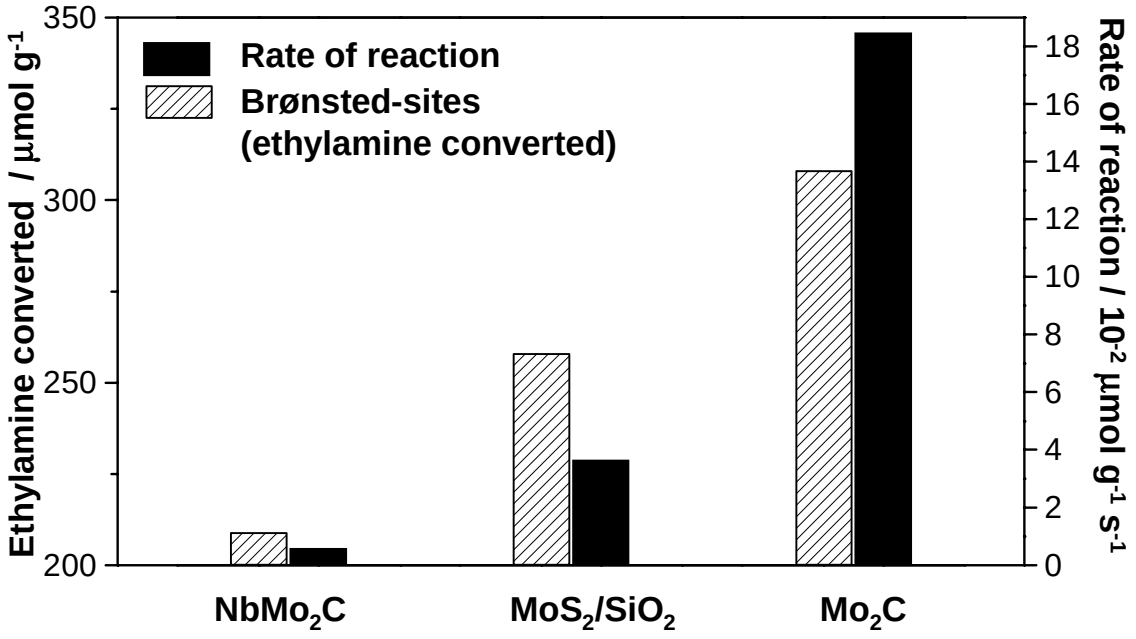


**Figure 4.9.** Relationship between the number of moles of ethylamine converted during TPD and the specific rate of reaction of *ter*-pentylamine on $Mo_2C$, $NbMo_2C$, and $MoS_2/SiO_2$.

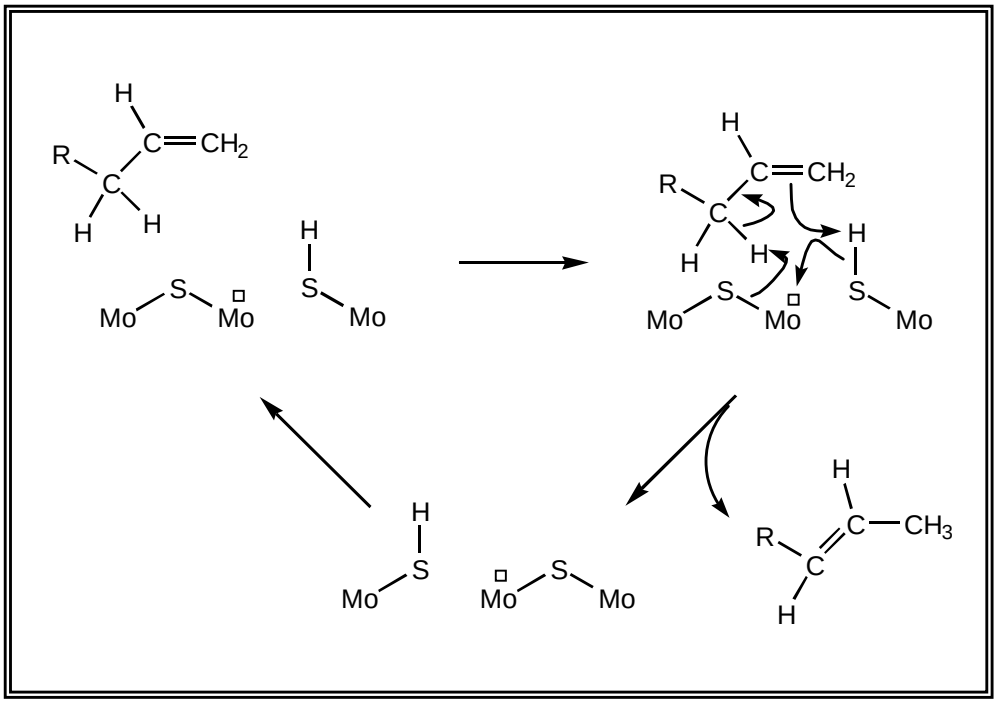


**Scheme 4.5.** Mechanism proposed for the isomerization of olefins.

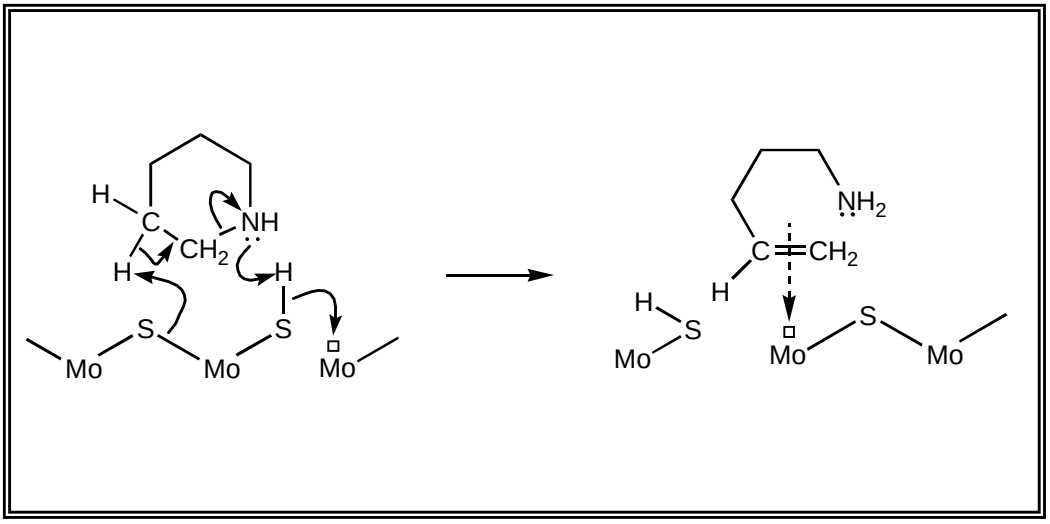


**Scheme 4.6.** Mechanism for initial HDN of cyclic amines.

Concerning the nature of the catalytic centers on the carbides, the results are qualitatively similar to those on a sulfide and a similar model could be speculated to occur on all these materials. It is very likely that the surface of the carbide upon exposure to $H_2S$, would be modified by sulfur to form a carbosulfide [45]. The surface would then contain the two types of sites cited before: Brønsted acid centers associated with sulfur atoms and nucleophilic sulfur ions.

Finally, comparison of the turnover rates of the carbides and sulfide catalyst offers another interesting point of discussion regarding the appropriate choice of measuring active sites. The overall rate of reaction of the isomeric amines is represented in Figure 4.10. The catalysts are compared on the basis of turnover rate, i.e., the number of product molecules produced per surface site per second. The number of surface sites is traditionally estimated by CO chemisorption [11,12,52,53] for the carbides and $O_2$ chemisorption [28,29,54] for the sulfides. On this basis (Figure 4.10a), $MoS_2/SiO_2$ is the most active of the series and $NbMo_2C$ is the least active. However, a good agreement between the specific rate of the catalysts for the *tert*-pentylamine reaction and the number of Brønsted-acidic sites (Figure 4.9) was obtained, suggesting that the ethylamine TPD technique should be more appropriate for comparison of catalytic activities on C-N bond cleavage reactions. Figure 4.10b shows the activity sequence determined on the basis of the number of active sites titrated by ethylamine TPD (Figure 4.7). The number of sites was measured by the number of moles of ethylamine converted to ethylene and ammonia (Brønsted sites). In this case, the activity of $Mo_2C$ for the *tert*-pentylamine and *n*-pentylamine reactions is substantially higher than that of the other catalysts, and slightly lower than the activity of $MoS_2/SiO_2$ for the *neo*-pentylamine reaction. Again, $NbMo_2C$

is the least active among all catalysts. This fact leads us to another point of discussion, which is the influence of the N-containing molecule on the catalytic activity. $NbMo_2C$ showed excellent levels of HDN conversion of quinoline (Table 4.3), being even superior to $Mo_2C$, whereas the sulfide catalyst presented a very low activity for the HDN of quinoline. This is because the HDN mechanism involves not only C-N bond cleavage of the aliphatic amine, but also requires hydrogenation of the heterocyclic amine and ring opening. As discussed earlier, even if the mechanism of HDN for heterocycles involves β-elimination, the site requirements for the consecutive reactions are probably more stringent. It is likely that the carbides (particularly $NbMo_2C$) are more effective than the sulfide at breaking C-N bonds in heterocyclic structures. Therefore, a more complete analysis is necessary in order to define the rate-determining step and properly compare the catalysts. This is the purpose of the next chapter.

a )

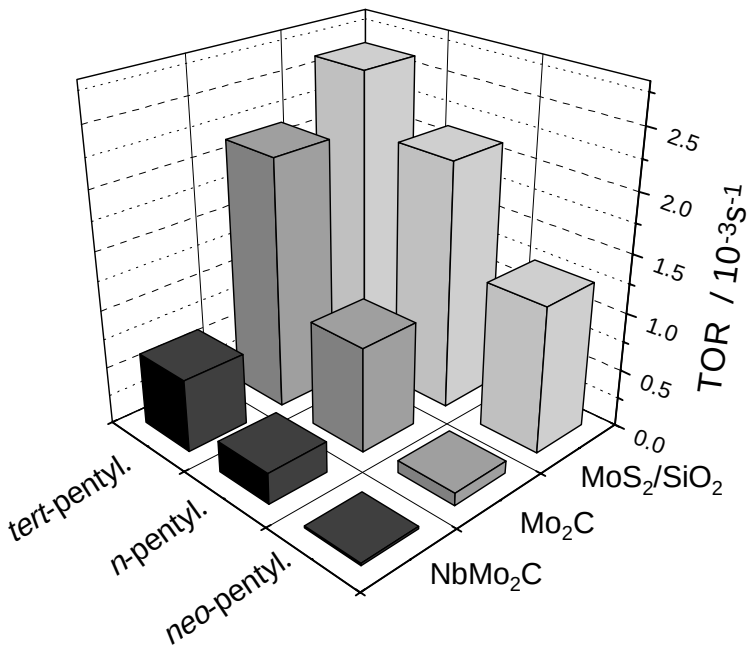


b )

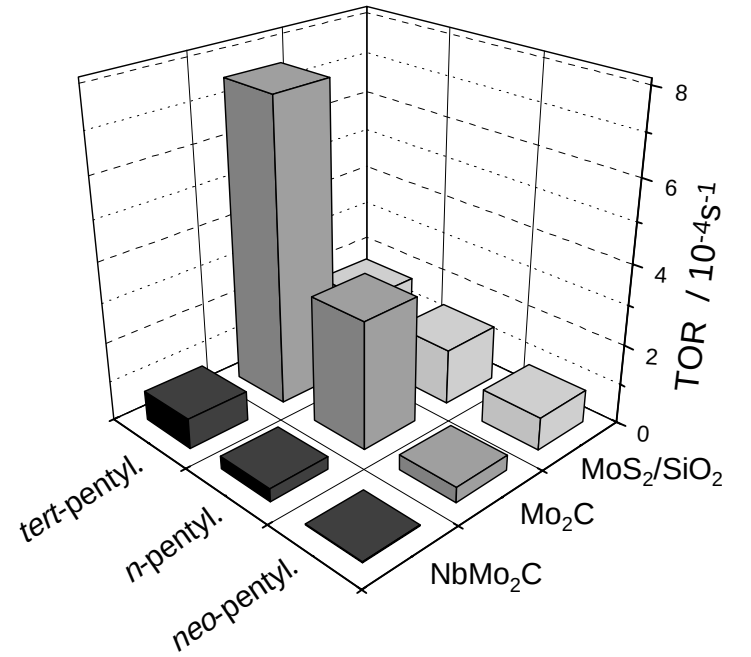


**Figure 4.10.** Overall turnover rates at 500 K of *tert*-pentylamine, *n*-pentylamine, and *neo*-pentylamine on $Mo_2C$, $NbMo_2C$, and $MoS_2/SiO_2$ based on the number of sites measured by: a) CO uptake for $Mo_2C$, $NbMo_2C$, and $O_2$ uptake for $MoS_2/SiO_2$ from Table 2; b) moles of ethylamine converted from Figure 8.

## 4.5. Conclusions

Our results suggest that a β-elimination is the main reaction pathway for amine bond cleavage over carbide and sulfide catalysts, since representative catalysts presented the same trend of activity, with *tert*-pentylamine being the most reactive amine, *n*-pentylamine being intermediate, and *neo*-pentylamine being the least reactive. TPD of ethylamine was demonstrated to be an appropriate technique for counting the number of Brønsted-acidic sites and for comparing catalytic activities for C-N bond cleavage reactions. The catalysts presented different ranges of activities for the C-N bond cleavage of aliphatic amines, nevertheless the product distribution was similar. Based on the similar results obtained for the carbide and sulfide catalysts, it is deduced that a similar surface composition is attained during reaction, a carbosulfide, giving rise to the same mechanism on the two catalyst classes for the deamination reaction. The mechanism is based on a push-pull process by basic sulfide centers and acidic-sulfhydril groups of Brønsted-acidic character. The sulfide centers on the carbide catalysts are probably formed upon exposure to $H_2S$, resulting in the formation of the carbosulfide surface structure.

**References**


[1] A. Stanislau, B.H. Cooper, Catal. Rev.-Sci. Eng. 36:1 (1994) 75.

[2] H. Topsøe, B.S. Clausen, F.E. Massoth, Hydrotreating Catalysis, Science and Technology, Springer, New York, 1991.

[3] P. Grange, X. Vanhaeren, Catal. Today 36 (1997) 375.

[4] S. Eijsbouts, Appl. Catal. A 158 (1997) 53.

[5] D.D. Whitehurst, T. Isoda, I. Mochida, Adv. Catal. 42 (1998) 345.

[6] S.T. Oyama in S.T. Oyama (Ed.), The Chemistry of Transition Metal Carbides and Nitrides, Blackie Academic and Professional, London, 1996, p.1.

[7] M. Nagai, T. Miyao, T. Tuboi, Catal. Lett. 18 (1993) 9.

[8] G.M. Dolce, P.E. Savage, L.T. Thompson Energy Fuels 11 (1997) 668.

[9] M. Nagai, A. Irisawa, S. Omi J. Phys. Chem. B 102 (1998) 7619.

[10] D.J. Sajkowski, S.T. Oyama, Appl. Catal. A 134 (1996) 339.

[11] S. Ramanathan, C.C. Yu, S.T. Oyama, J. Catal. 173 (1998) 10.

[12] C.C Yu, S. Ramanathan, B. Dhandapani, J.G. Chen, S.T. Oyama, J. Phys. Chem. B, 101 (1997) 512.

[13] N. Nelson, R.B. Levy, J. Catal. 58 (1979) 485.

[14] J.L. Portefaix, M. Cattenot, M. Guerriche, J. Thivolle-Cazat, M. Breysse, Catal. Today 10 (1991) 473.

[15] M. Cattenot, J.L. Portefaix, J. Afonso, M. Breysse, M. Lacroix, G. Perot, J. Catal. 173 (1998) 366.

[16] T.C. Ho, Catal. Rev.-Sci. Eng. 30:1 (1988) 117.

[17] F. Goudriaan, H. Gierman, J.C. Vlugter, J. Inst. Petrol. 59:565 (1973) 40.

[18] C.N. Satterfield and S. Gültekln, Ind. Eng. Chem. Proc. Des. Dev. 20 (1981) 62.

[19] R.T. Hanlon, Energy Fuels 1 (1987) 424.

[20] R.M. Laine, Catal. Rev.-Sci. Eng. 25 (1983) 459.

[21] J.L. Portefaix, M. Cattenot, M. Guerriche, M. Breysse, Catal. Lett. 9 (1991) 127.

[22] V. Schwartz, V.T. da Silva, J.G. Chen, S.T. Oyama, Proc. 12th Int. Cong. Catal., Granada, Spain (2000), in press.

[23] S.T. Oyama, C.C. Yu, S. Ramanathan , J. Catal. 184 (1999) 535.

[24] V. Schwartz, J.G. Chen, S.T. Oyama, Proc. 215th National Meeting, ACS Division of Petroleum Chemistry, Dallas, TX (1998).

[25] V. Schwartz, J.G. Chen, S.T. Oyama, Proc. 16th North American Catalysis Society Meeting, Boston, MA (1999).

[26] T.P. St. Clair, B. Dhandapani, S.T. Oyama, Catal. Lett. 58 (1999) 169.

[27] V.T. da Silva, M. Schmal, S.T. Oyama, J. Sol. St. Chem. 123 (1996) 168.

[28] W. Zmierczak, G. MuraliDhar, F.E. Massoth, J.Catal. 77 (1982) 432.

[29] T.A. Bodrero, C.H. Bartholomew, J.Catal. 78 (1982) 253.

[30]H.M. McNair, J.M. Miller, Basic Gas Chromatography, John Wiley & Sons, New York, 1998, p. 135.

[31] S.T. Hadden, H.G. Grayson, Hydrocar. Proc. Petrol. Refin. 40 (1961) 207.

[32] C.L. Yaws, Thermodynamic and Physical Property Data, Gulf Publishing Company, Texas, 1992, p. 151.

[33] S.W. Benson, Thermochemical Kinetics, Wiley, New York, 1969, Chap. 2.

[34] D.J. Parillo, A.T. Adamo, G.T. Kokotailo, R.J. Gorte, Appl. Catal. A 67 (1990) 107.

[35] C. Pereira, R.J. Gorte, Appl. Catal. A 90 (1992) 145.

[36] A.G. Palkhiwala, R.J. Gorte, Catal. Lett. 57 (1999) 19.

[37] D. Zeroka, J.O. Jensen, A.C. Samuels, J. Molec. Struct. 465 (1999) 119.

[38] H. Hagemann, H. Bill, J. Chem. Phys. 80 (1984) 111.

[39] D. Lin-Vien, N.B. Colthup, W.G. Fateley, J.G. Grasselli, The Handbook of Infrared and Ramam Characteristic Frequencies of Organic Molecules, Academic Press, California, 1991, Chap. 10.

[40] J. Sonnemans, P. Mars, J. Catal. 34 (1974) 215.

[41] H. Schulz, M. Schon, N.M. Rahman in L. Cerveny (Ed.), Studies in Surface Science and Catalysis, Elsevier, Amsterdam, 1986, Vol. 127, Chap. 6.

[42] M. Danot, J. Afonso, J.L. Portefaix, M. Breysse, T. des Courieres, Catal. Today 10 (1991) 629.

[43] P.A. Aegerter, W.W.C. Quigley, G.J. Simpson, D.D. Ziegler, J.W. Logan, K.R. McCrea, S. Glazier, M.E. Bussell, J. Catal. 164 (1996) 109.

[44] J.A.R. Van Veen, J.K. Minderhoud, J.G. Buglass, P.W. Lednor, L.T. Thompson, Mat. Res. Soc. Symp. Proc., 368 (1995) 51.

[45] B. Dhandapani, T. St.Clair, S.T. Oyama, Appl. Catal. A 168 (1998) 219.

[46] R.R. Chianelli, G. Berhault, Catal. Today 53 (1999) 357.

[47] R.T. Morrison, R.N. Boyd, Organic Chemistry, 6$^{th}$ Edition, Prentice Hall, New Jersey, 1992, p. 308

[48] L. Vivier, V. Dominguez, S. Kaztelan, G. Perot, Catal. Today 10 (1991) 156.

[49] S.H. Yang, C.N. Satterfield, J. Catal. 81 (1983) 168.

[50] S.H. Yang, C.N. Satterfield, Ind. Eng. Chem. Proc. Des. Dev. 23 (1984) 20.

[51] G. Berhault, M. Lacroix, M. Breysse, F. Maugé, J.C. Lavalley, H. Nie, L. Qu, J. Catal. 178 (1998) 555.

[52] J.S. Lee, K.H. Lee, J.Y. Lee, J. Phys. Chem. 96 (1992), 362.

[53] K.R. McCrea, J.W. Logan, T.L. Tarbuck, J.L. Heiser, M.E. Bussel, J. Catal. 171 (1997) 255.

[54] S.J. Tauster, T.A. Pecoraro, R.R. Chianelli, J. Catal. 63 (1980) 515.